Molecular simulations of lubrication and solvation forces

Sivakumar R. Challa*
Department of Chemical and Nuclear Engineering, Center for Micro-Engineered Materials, The University of New Mexico/NSF, Albuquerque, New Mexico 87106, USA

Frank van Swol†
Sandia National Laboratories, Albuquerque, New Mexico 87185, USA
(Received 14 September 2005; published 26 January 2006)

We report on molecular-dynamics simulations of the drag force experienced by a smooth sphere as it approaches a smooth planar surface to test the predictions of classical hydrodynamic theory. We use a simple repulsive Lennard-Jones-like model to represent the fluid interactions, and calculate the total force on the sphere as a function of its radius, velocity, and distance from the surface. We find that the presence of static solvation forces complicates the testing of hydrodynamic theory which predicts a divergent repulsive lubrication force as the gap vanishes. The solvation force contribution is most prominent at small gaps and small velocities. For a smooth wall its presence can lead to a total force that is oscillating between positive and negative, quite different from the hydrodynamic prediction. To enable an improved test of the lubrication predictions, we propose a different approach that measures the total force for approaching as well as receding spheres. We suggest a simple general analysis that decouples the dynamic and static force contributions on the sphere. The new decoupling method is applicable to simulations and laboratory experiments alike. We illustrate its power by applying it to the molecular-dynamics data.

DOI: 10.1103/PhysRevE.73.016306 PACS number(s): 47.15.G−

I. INTRODUCTION

A particle moving through a viscous fluid is subject to a drag that resists the motion. The drag force is an increasing function of the particle's velocity U, and it can be determined experimentally from a settling experiment by measuring the terminal velocity. Indeed, for a spherical particle this measurement provides the traditional route to the fluid viscosity. It uses a result due to Stokes [1], who applied hydrodynamic theory under conditions of creeping flow to show that the drag force is proportional to the sphere's radius b and the fluid viscosity μ. Hence the force is commonly known as Stokes drag or Stokes' law. If the sphere falls toward a planar wall, the drag force also becomes a function of the separation, h, from the wall. Well away from the wall the drag force approaches Stokes drag, but the drag force increases rapidly close to the wall. An analytical solution to this well-known hydrodynamics problem was first provided by Brenner in 1961. Brenner's solution [2] exhibits a divergence (as $1/h$) in the limit that $h \to 0$. The divergence is, of course, inherent to the underlying approximations made in the continuum hydrodynamics, among which is the assumption that the fluid is a continuum with a spatially constant density. However, we certainly know that at a small enough length scale there will come a point where the fluid density will display the signs of its particulate nature. That is, if the gap between the sphere and the wall is reduced to molecular size, σ, we expect the hydrodynamic solution to become unphysical, even for a perfectly smooth sphere. The natural questions to be asked therefore include the following: what is the precise nature of the breakdown of hydrodynamics, at what length scale can it be observed, and how can we measure this in an experimental situation?

Several years ago, Vergeles *et al.* [3,4], following in the footsteps of Alder *et al.* [5], set out to use molecular dynamics (MD) to address the first two questions. Vergeles *et al.* performed a detailed study of both the translational and rotational motion of a single sphere in a Lennard-Jones (LJ) fluid as it approaches a planar wall. These authors concluded that the MD simulations confirmed the hydrodynamic predictions away from the wall, while close to the wall the unphysical divergence is removed.

An issue that was not addressed by Vergeles *et al.* [3,4], and which prompted the simulations reported here, concerns the role played by the solvation force that acts between any two surfaces immersed in a fluid. The solvation force has a purely thermodynamic origin. It is a derivative of a surface free energy with respect to separation and acts at equilibrium. It can and has been measured in a simulation and calculated from liquid state theories of inhomogeneous fluids (e.g., [6,7]). Solvation forces can also be probed with a surface force apparatus (SFA) [8], an atomic force microscope (AFM), or the interfacial force microscope (IFM), which directly measure the force versus separation curve between two surfaces. In addition, the more indirect method of osmotic stress measurements provides information about the solvation force acting between arrays of macromolecules in solution [9].

The form and the range of the solvation force [10] can vary widely depending on the nature of the solution as well as that of the surface. For instance, the interaction between

*Email address: challa@unm.edu
†Email address: vanswol@unm.edu; Department of Chem. and Nuclear Eng., Center for Micro-Engineered Materials, the University of New Mexico/NSF, Albuquerque, NM 87106.

two similarly charged surfaces in an aqueous solution is repulsive and electrostatic in origin. Its characteristic range is set by the Debye screening length, which strongly depends on the ionic strength of the solution. The interaction range is large (short) for low (high) ionic strength, and is often well-described by Derjaguin, Landau, Verwey, and Overbeek (DLVO) [8] theory. Two hydrophobic surfaces can also interact over large distances up to a μm via an attractive force. Finally, in a molecular fluid composed of roughly spherical molecules [e.g., water, argon, octamethylcyclotetrasiloxane (OMCTS)], one observes a short-ranged force that is, if the opposing surfaces are sufficiently smooth, oscillating between repulsive and attractive on the scale of σ.

Therefore, for a sphere that is slowly moving through a molecular fluid and closely approaching a planar wall, one must expect to measure a force that resembles the solvation force. Indeed, in the limit that $U=0$, one obtains the solvation force exactly. This observation contrasts with the hydrodynamic prediction (Brenner), which approaches zero in that limit. At higher velocities one expects to see a signature of the solvation force (as indicated by the results of Vergeles *et al.*) but now the solvation force is coupled with the velocity-dependent dynamic contribution of the kind described by Brenner.

The presence of the solvation force implies that any comparison of fluid drag between a molecular simulation and hydrodynamics must address the dependence on U. The same conclusion applies to an SFA, AFM, or IFM experiment.

We start our article by outlining the salient hydrodynamic relations, and describing the details of our MD simulations in the next two sections. The simulation results of fluid drag force for various cases will be presented in the subsequent section with an analysis of a drag force decomposition that reconciles the solvation force and the hydrodynamic force in an intuitively logical manner, and which can equally be applied in experimental investigations.

II. HYDRODYNAMICS

The case of a sphere moving toward a planar wall is, of course, a well-known problem in hydrodynamics. In 1961, Brenner provided the analytical solution for the force on such a sphere of radius b, with its leading edge a distance h away from the wall as it moves at a velocity U through a fluid of viscosity μ,

$$F_B = 6\pi\mu b U\lambda, \tag{1}$$

where $\lambda=\lambda(h/b)$ is given by

$$\lambda = \frac{4}{3}\sinh\alpha\sum_{n=1}^{\infty}\frac{n(n+1)}{(2n-1)(2n+3)} \times\left[\frac{2\sinh(2n+1)\alpha+(2n+1)\sinh 2\alpha}{4\sinh^2(n+1/2)\alpha-(2n+1)^2\sinh 2\alpha}-1\right], \tag{2}$$

and where we used the following shorthand notation:

$$\alpha = \cosh^{-1}(h/b+1). \tag{3}$$

Thus, far away from the wall ($h\to\infty$), the sphere experiences a constant force (Stokes drag),

$$F_S = 6\pi\mu b U \tag{4}$$

while in the opposite limit, close to the wall, the force diverges as $1/h$,

$$F_B \to 6\pi\mu b^2 U/h. \tag{5}$$

III. SIMULATION METHODS

The MD simulations were performed with a rectangular box (of dimensions $L_x\times L_y\times L_z, L_x=L_y$,) with periodic boundaries applied to the x and y directions while a pair of parallel walls was placed perpendicular to the z direction. The fluid particles have a mass m, and interact via a pair potential. For the fluid-fluid interaction potential, we chose the Week, Chandler, and Andersen (WCA) potential [11], which is a cut and shifted 12-6 LJ potential cut at the minimum $r_c/\sigma=2^{1/6}\approx 1.122$,

$$\phi(r_{ij}) = \begin{cases}\phi_{12\text{-}6}(r)-\phi_{12\text{-}6}(r_c), & r<r_c\\ 0, & r>r_c,\end{cases} \tag{6}$$

where $r_{ij}=|\mathbf{r_i}-\mathbf{r_j}|$ denotes the scalar distance between particles i and j and

$$\phi_{12\text{-}6}(r) = 4\epsilon\left[\left(\frac{\sigma}{r}\right)^{12}-\left(\frac{\sigma}{r}\right)^{6}\right]. \tag{7}$$

The parameters ϵ and σ are used as the basic units of energy and length, respectively. Velocities will be reported in units of $\sqrt{\epsilon/m}$ and time in units of $\sqrt{m\sigma^2/\epsilon}$. This particular intermolecular potential [Eq. (6)] is extremely convenient because it is short-ranged, is purely repulsive, has a zero force at the cutoff, and is known to give an excellent representation of the structure and dynamics of the full LJ potential.

Each of the planar walls acts as a one-body external field on the fluid. For this particular finite-ranged interaction we use an integrated LJ potential, namely a cut and shifted 9-3 potential, viz.,

$$V_{\text{ext}}(z) = \begin{cases}\phi_{\text{wf}}(z)-\phi_{\text{wf}}(z_c), & z<z_c\\ 0, & z>z_c,\end{cases} \tag{8}$$

where $z=|z_i-z_w|$ denotes the distance of particle i from a wall (located at $z_w=0$ and $z_w=L_z$), and

$$\phi_{\text{wf}}(z) = \epsilon_{\text{wf}}(2/5)^{1/2}\left[\frac{1}{5}\left(\frac{\sigma}{z}\right)^9-\frac{3}{2}\left(\frac{\sigma}{z}\right)^3\right]. \tag{9}$$

The value of the cutoff is set at $z_c/\sigma=2.5$ and this gives the external field a short-ranged attraction.

The potential between the fluid particles and the suspended sphere of diameter d is spherically symmetric and given by a modified WCA potential. That is,

$$\phi_{\mathrm{sf}}(r) = \begin{cases} \phi_{12\text{–}6}(r - d/2) - \phi_{12\text{–}6}(r_c), & r < r_c + d/2 \\ 0, & r > r_c, \end{cases} \tag{10}$$

where r is the distance between a fluid particle and the center of the sphere and the shifted argument $r-d/2$ indicates that potential is acting from the surface of the sphere. Note that we use the same value for r_c as for the fluid-fluid interaction, which implies that ϕ_{sf} is again purely repulsive. Also, for a point-sized sphere ($d=0$) the sphere-fluid potential reduces to the fluid-fluid potential.

Finally, for the interaction between the sphere's surface and the wall we simply employ a hard-wall potential,

$$\phi_{\mathrm{ws}}(z) = \begin{cases} \infty, & z < 0 \\ 0, & z > 0. \end{cases} \tag{11}$$

Thus, the closest approach of the center of a sphere from $z_w=0$ or $z_w=L_z$ is $d/2$, at which time a hard-sphere collision is performed for the sphere by simply reversing the direction of the sphere's velocity. The above choice was made entirely for simplicity. The wall contribution to the total force on the wall is simply additive; thus, any other functional form for the wall-sphere interaction that one would like to consider can be simply added to the results presented below.

It is worth stressing that the details of the potentials used here are not expected to affect the results of the drag force in any significant way. As mentioned, the WCA fluid is very similar in structure to a LJ fluid at the same density and temperature. Similarly, the range or strength of the sphere-fluid interaction should not affect the Stokes drag. All one aims for is that the wall-fluid and sphere-fluid potentials are conducive for wetting by the fluid.

A typical simulation was started by implanting a sphere of diameter d inside a regular fcc crystal lattice of WCA particles, removing those particles that overlapped with the implanted sphere. Following Vergeles *et al.* [3,4], the crystal density was set at $\rho\sigma^3=0.8$, and the starting system was then prepared by first melting the crystal at a high temperature and then equilibrating at the final temperature of $kT/\epsilon=1.2$. The simulations were run in the NVT ensemble using the Hoover-Nose thermostat to keep the temperature constant [12].

The sphere was set moving in the z direction at a constant velocity U, which is equivalent to setting the sphere's mass to infinity. During a run we calculate the z component of the total force on the sphere exerted by the fluid particles and collect the data in a histogram of width approximately 0.05σ to create a force profile. Typically, the initial position of the sphere is at one end of the box, touching (or almost touching) the nearest wall while set to move toward the other end. Most runs ended when the opposite wall was reached, but in some cases we continued the run after the sphere performed a hard-sphere collision with the target wall.

In order to analyze the data, and to compare the force on the sphere with the hydrodynamic prediction, we require the viscosity of the bulk fluid at $kT/\epsilon=1.2$ and $\rho\sigma^3=0.8$. Various simulation strategies are available to determine the viscosity [12]. We elected to perform a separate set of bulk simulations in a cubical box to generate the stress-stress correlation function. Following the Green-Kubo formalism [11], we extracted the viscosity to obtain $\mu\sqrt{m\epsilon}/\sigma^2=1.74$. We use this value throughout this paper. We also note that the falling sphere simulations themselves can serve as an independent check on the value of μ as in the bulk we should recover Stokes' law.

TABLE I. Simulation details.

N	L_x/σ	L_z/L_x	d/σ	b
4002	13.68	2	4	3
32328	27.36	2	8	5
32018	27.19	2.5	10	6
213880	51.3	2	15	8.5

IV. RESULTS

Simulations were run for four different sphere sizes. In terms of the fluid particle diameter these are $d/\sigma=4$, 8, 10, and 15. As the sphere size increases, the number of fluid particles, N, needs to grow as well to ensure a sufficiently large simulation box such that there is no significant interaction between the images of the sphere and the interfacial regions near the walls. The pertinent details have been collected in Table I.

To compare our MD results with the hydrodynamic predictions [i.e., Eq. (1)], we have to assign a parameter, b, to the radius of the falling sphere, and a parameter, h, to the separation between the sphere's surface and the planar wall. In molecular systems size is not a uniquely defined quantity; it is the interaction potentials and the temperature combined that determine how close two fluid particles, or a fluid particle and a sphere, or a sphere and a wall can approach.

The smallest possible separation between the center of a fluid particle and the center of the sphere is exactly $d/2$, but this is not necessarily a good indication of the size. Since the interaction potential [Eq. (10)] rises very steeply when the separation is less than $\approx d/2+\sigma$, the corresponding Boltzmann factor, $\exp(-\phi_{\mathrm{sf}}/k_BT)$, is so small that such a separation is hardly ever observed. In practice, the smallest observed separation is roughly $d/2+\sigma$, and throughout this paper we will follow Vergeles *et al.* [3,4] and settle on the identification $b=d/2+\sigma$ [13]. Liquid state perturbation theory [11] has developed more sophisticated criteria for assigning an effective hard-sphere diameter to particles interacting via soft potentials. For the present conditions, such a calculation would give no significant change, i.e., we obtain $b=d/2+1.0056\sigma$. For typical liquid state conditions, the more sophisticated value for $b-d/2$ can be expected to be within 3% of σ.

Since the sphere and the wall interact via an infinitely hard and perfectly short-ranged potential, the distance between the wall and the sphere is well-defined. That is, the smallest distance between the sphere's surface and the wall is zero, and this coincides with our interpretation of h. We recognize that an alternative definition of h would result if we

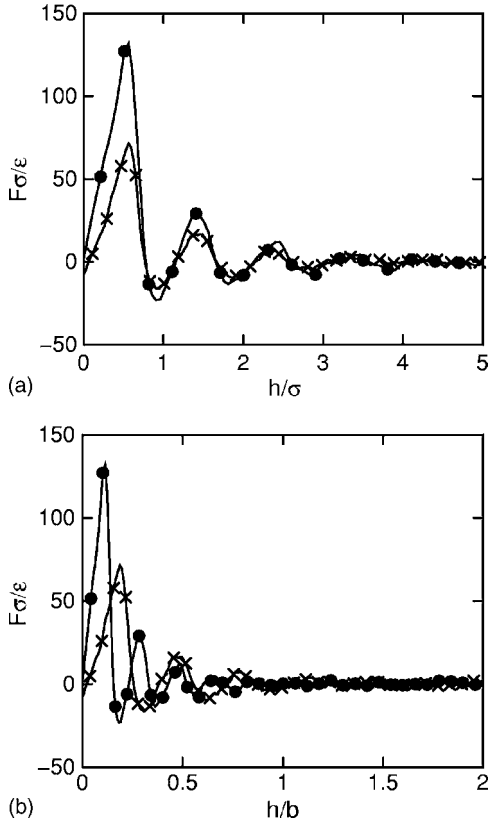

FIG. 1. The solvation force (i.e., $U=0$) as a function of separation. The results shown are for $d=4$ or $b=3$ (cross) and $d=8$ or $b=5$ (circle). In (a) we plot versus h/σ, while in (b) we plot the same data versus h/b. For clarity, only a few points are highlighted with symbols in all the figures.

generalize the viewpoint expressed above, when defining b. That interpretation would identify h as the distance between two equipotential surfaces for the fluid, that is, one potential surface located at $z=\sigma$ (and for the opposing wall at $z=L_z-\sigma$) and one associated with a radial distance $r=d/2+\sigma$ from the sphere's center. Such a choice would differ from our hard-sphere/hard-wall choice by 2σ.

Clearly, the degree in arbitrariness of the definitions of h and b is intrinsic to molecular systems and thus has to be accepted. It equally affects the comparisons presented here as those reported in AFM studies.

We first present the results for the solvation force (F_{solv}), that is, the force on the sphere when $U=0$. In Fig. 1, we plot the total force ($F\sigma/\epsilon$) on the sphere as a function of the dimensionless separation. We display the data in two different ways, as a function of h/σ [Fig. 1(a)] and as a function of h/b [Fig. 1(b)]. The data represent force curves typically found for a one-component fluid confined between a smooth planar wall and a smooth sphere. Each force data point, at a particular dimensionless separation, is an average of F_z obtained from a simulation of a stationary sphere conducted over 20000 time steps (100 time units.) The data points are spaced equally with a separation of 0.05σ, and the entire force curve is smoothed using a Savitzky-Golay smoothing filter [14]. The force oscillates between positive (repulsive) and negative (attractive) with a period that closely reflects the molecular size of the fluid particles, σ, and with an amplitude that decreases with h. Note that the solvation force displays attractions even though the fluid-fluid interaction itself is purely repulsive. Figure 1(a) shows that the amplitude of the oscillations increases with sphere size, in accordance with the Derjaguin approximation, which predicts that the force is proportional to the sphere diameter [8]. The two curves remain perfectly in phase with each other. Figure 1(b) highlights the effects of plotting the data versus h/b, the natural hydrodynamic separation variable. As the sphere size increases, the oscillations become more rapid on the h/b scale, but interestingly the maxima and minima each appear to share a common envelope. The solvation force found here from a simulation can be compared directly to both SFA measurements [8] as well as AFM measurements.

The nonzero force on the sphere for $U=0$ is the first and perhaps clearest indication that the hydrodynamics result is expected to be incorrect for the case of small velocities and small sphere-wall separations. Our system, consisting of smooth planar walls, a smooth sphere, and a one-component fluid, displays the strongest signature of the structure and interactions of the fluid confined to the gap between the sphere and the wall. The pronounced layering of the fluid particles that gives rise to the pronounced force oscillations is known to be strongly affected by molecular surface roughness. However, some years ago Frink and van Swol [7] have demonstrated that surface roughness does not lead to a cancellation or "washing out" of the solvation force. Rather, for typical wetting surfaces such as the ones used here, the solvation force for a rough surface was found to exhibit a broad purely repulsive feature. Only at very small separations does an attraction survive due to completely empty parts of the gap. Within a superposition approximation the solvation force for a rough surface can be written simply as a weighted average over the smooth surface solvation force. For example, for a slitlike gap the average over a gap with rough surfaces is an average over different local separations of smooth gaps, and hence $F_{\mathrm{solv}}^{\mathrm{rough}}(\bar{h})$ can be conveniently expressed in terms of a normalized probability density distribution, $\mathcal{P}_r(h;\bar{h})$, of local separations (see [7]),

$$F_{\mathrm{solv}}^{\mathrm{rough}}(\bar{h}) \approx \int_0^\infty dh' F_{\mathrm{solv}}^{\mathrm{smooth}}(h')\mathcal{P}_r(h';\bar{h}), \qquad (12)$$

where $\bar{h}$ denotes the nominal gap size of a slit with rough surfaces. From this we can see that the reason for the noncancellation of attractions and repulsions lies therefore in the presence of the first strong peak, which is repulsive (and associated with squeezing out the very last molecular layer) and the decaying amplitude of the extrema in the force. For a detailed analysis with explicit examples, we refer the reader to Ref. [7]. In summary, molecular roughness can strongly affect the appearance of the solvation force, but typically not its presence [15] altogether.

We now turn our attention to a small but nonzero value of U. In Fig. 2, we present the drag force [16] results for $U=0.01$ and $b=3$. This corresponds to a Reynolds number, Re, well below 1, namely $\mathrm{Re}=\rho Ub/\mu=0.014$. The force curves

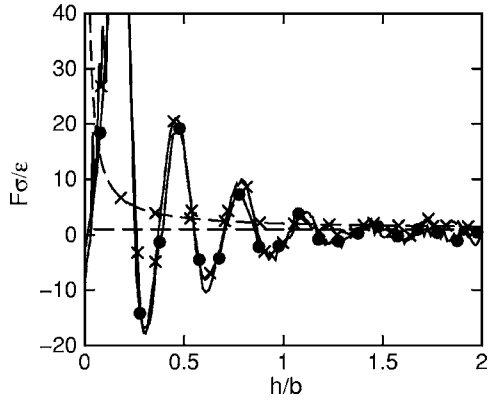

FIG. 2. The drag force (solid curve with crosses) as a function of separation at $U=0.01$ for $b=3$. The solid curve with circles represents the associated solvation force, the broken line represents the Stokes drag, while Brenner's result, Eq. (1), is shown as a broken curve with crosses.

for nonzero sphere velocities are obtained by averaging over 20 simulations, each of which starts at the same separation from the wall but with a different particle configuration. The force points themselves are averaged over a distance of 0.05σ in a simulation. As mentioned earlier, curve smoothing has been employed for presenting the figures. It is clear that the hydrodynamic prediction, Eq. (1), performs poorly, whenever it deviates substantially from the large h limit, i.e., simple Stokes drag. The drag force appears essentially as shifted upward from the equilibrium solvation force. This suggests that for sufficiently small U, the measured drag force can be interpreted as a simple superposition of two contributions. One is an h-dependent "static" force (i.e., solvation force) and the other is a dynamic contribution that depends on both h and U, viz.,

$$F(U;h) = F(0;h) + F_{\mathrm{dyn}}(U;h). \tag{13}$$

The results for a larger velocity of the sphere are shown in Fig. 3, where we plot the drag force for $U=0.2$ and $b=3$. The above-suggested superposition still seems to be useful as a guide, although for $h/b>1$ the measured force is somewhat above F_{solv} but not quite as high as F_B. Clearly, with increas-

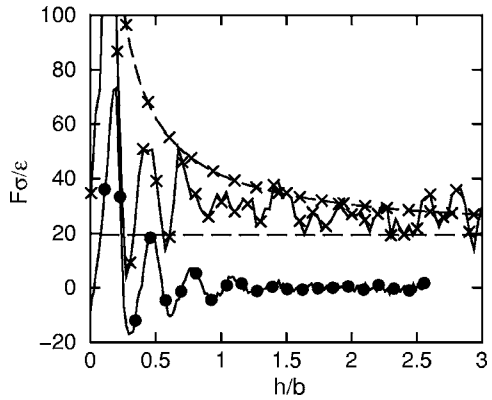

FIG. 3. The drag force (solid curve with crosses) as a function of separation at $U=0.2$ for $b=3$. Symbols are the same as in Fig. 2.

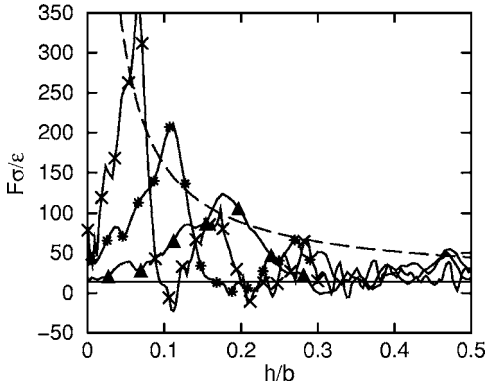

FIG. 4. The drag force (solid curves) as a function of separation at Re=0.1954 for varying sphere sizes: $b=3$ (triangle), $b=5$ (asterisk), and $b=8.5$ (cross). Thin solid curve represents the Stokes drag, while the broken curve represents Brenner's prediction.

ing U the Brenner expression starts to overpredict the drag force. We note that much larger values of Re are not really accessible for a sphere of this size. The average speed of a fluid particle is given by $\sqrt{8kT/(m\pi)} \approx 1.75\sqrt{\epsilon/m}$ for our temperature, $kT/\epsilon=1.2$. The isothermal speed of sound is approximately $5.6\sqrt{\epsilon/m}$. When the sphere velocity approaches the average fluid particle speed, local heating will start to play a considerable role and one cannot expect simple isothermal fluid flow to persist.

To study the effect of sphere size, we simulated spheres with diameter varying from 4 to 15 (see Table I). The Reynolds number was kept constant at Re=0.1954 while varying the sphere size and velocity reciprocally. Thus, Brenner's prediction should be the same for all sphere sizes, as should the Stokes drag. However, this is not observed in the simulation results close to the surface. An example of the results is shown in Fig. 4. We see from this figure that the discrepancy between the measured drag force and Brenner's prediction does not diminish with increasing diameter.

We will now consider a sphere moving away from a wall with a velocity U. Within hydrodynamic theory this does not present anything new: the drag force, Eq. (1), merely changes sign, now pointing toward the wall (see Fig. 5). Thus, within hydrodynamics the drag force is antisymmetric: positive (repulsive) when moving toward the wall, and negative (attractive) when moving away. We find that the molecular-dynamics results are qualitatively quite different from this picture (see Fig. 5) near the wall (i.e., $h/b<1$.) We observe that when the sphere moves outward it experiences a drag force that is not merely the negative of the drag force when moving toward the wall. Instead, the force is considerably less negative near the wall than antisymmetry would suggest. Therefore, we can conclude that antisymmmetry inherent to the hydrodynamic theory is not shared by the actual MD simulations.

The lack of antisymmetry indicates that the measured drag force near the wall contains a contribution that is independent of U [cf. Eq. (13)]. One can easily discern regularly spaced and proportionately decaying oscillations close to the wall, irrespective of the direction of motion of the sphere, that are reminiscent of solvation force oscillations. This

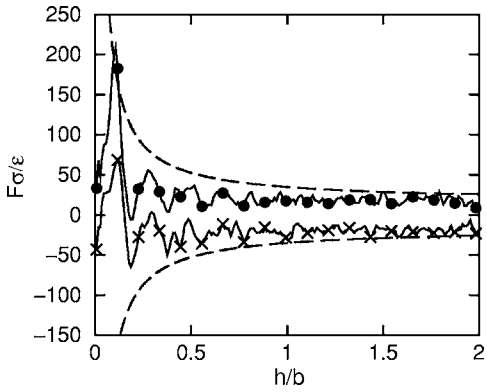

FIG. 5. The drag force as a function of separation for a sphere of size $b=5$ moving toward (and away from) a surface at $U=0.1$. The solid curve with crosses represents the force on the sphere while receding from the surface, and the solid curve with circles denotes the force while approaching the surface. The broken curves represent drag force from Brenner's prediction, the positive curve for the sphere approaching the surface and the negative curve for the receding sphere.

static contribution approaches the solvation force in the limit of small U, not presented here. The aforementioned superposition approximation suggests that by assuming that $F_{\mathrm{dyn}}(U;h)$ *is* antisymmetric, we can, in fact, extract a static and a dynamic component as follows:

$$F_{\mathrm{static}}(U;h) = \frac{1}{2}[F(U;h) + F(-U;h)], \tag{14}$$

$$F_{\mathrm{dyn}}(U;h) = \frac{1}{2}[F(U;h) - F(-U;h)]. \tag{15}$$

Defining the static force as a velocity-dependent function makes it slightly more general than a simple superposition approximation [17]. The static force [Eq. (14)] vanishes for large h, while the dynamic force [Eq. (15)] should approach a nonzero value, namely the Stokes drag [Eq. (4)]. The simulations presented in this paper provide a straightforward test of the decomposition approach. In Fig. 6, we present an example of the decomposition for $U=0.1$. We see that for this velocity, the suggested decomposition consitutes a very satisfactory approach, despite the considerable noise present. The static force F_{static} is clearly consistent with the solvation force, and the dynamic force displays the correct large h limit. We note that the dynamic force does not appear to be a strong function of h. F_{dyn} does not exhibit the strong upturn of Brenner's force very close to the wall.

We stress that the decoupling introduced here is specifically aimed at separating the solvation interaction from a hydrodynamic contribution, relying on the antisymmetric nature of the latter. Of course, in any (computer) experiment one may encounter situations where the approaching and retracting force curves differ for reasons other than strictly hydrodynamic interactions. This can occur, for instance, in AFM measurements using probes covered with compliant self-assembled monolayers. A computer modeling example can be found in a recent paper by Drazer *et al.* [18], who

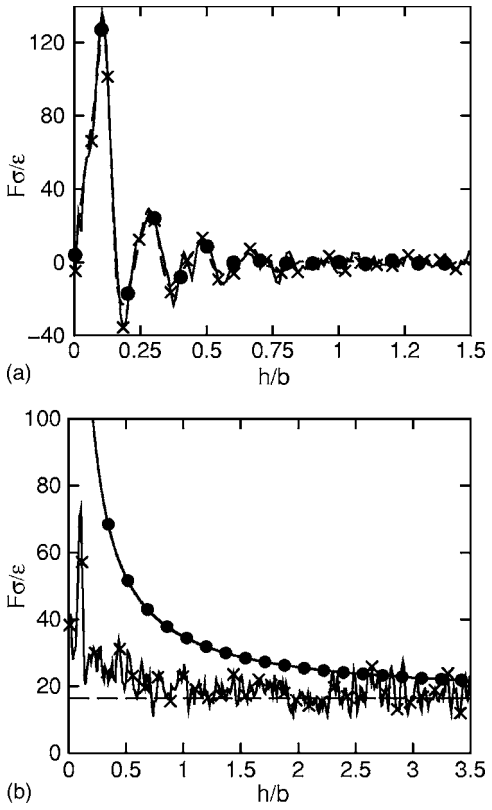

FIG. 6. The static (a) and the dynamic (b) component of the drag force as a function of separation for a sphere moving toward a wall with a velocity $U=0.1$. The results shown are for $b=5$. (a) Comparison of the static force (solid curve, cross) and the equilibrium solvation force (broken curve, circle). (b) Comparison of the dynamic force (solid curve, cross) and the Stokes (broken curve) and Brenner (solid curve, circle) predictions.

used molecular simulation to study nonequilibrium effects in the adhesion of nanoparticles to cylindrical walls. These authors report hysteresis between the approach of a spherical object toward a dynamic and compliant wall, and the subsequent pull-off. Using a quasistatic movement of the sphere to obtain the free-energy changes, Drazer *et al.* [18] obtained two force curves that clearly differ with the direction of the movement. Rather than a sign of hydrodynamic interactions, in this case, the direction dependence of the force likely points to the existence of metastable states. These metastable states cause the measured force to exhibit a history dependence [19].

V. DISCUSSION

In this paper, we have used MD to revisit the problem of a sphere moving toward a planar wall. The simulations demonstrate that the role of the equilibrium solvation force is an important one. The solvation force has a thermodynamic origin and is present at any velocity. But the solvation force becomes the dominant contributor to the measured drag force at small approach velocities (i.e., in the limit $U\rightarrow 0$) close to the surface. This is in marked contrast to hydrodynamic theory, which predicts a divergent drag force close to the surface.

The simulations presented in this paper primarily serve to illustrate the basic interplay between static and dynamic force contributions and were purposely kept extremely simple. Thus, no attempt was made to make the wall-fluid interactions more realistic by including molecular detail. However, Vergeles *et al.* [4] have presented data for both smooth and molecular walls. Very close to the wall (within 2σ) the resistance force is found to be strongly dependent on the wall details. However, by presenting the *total* force acting on the moving sphere (cf. Fig. 6 of Ref. [4]), it is not straightforward to interpret the observed differences. In principle, they could be attributed to a difference in the static (i.e., solvation) force, or they could point to differences between the dynamic contributions (e.g., slip versus no slip), or a combination of both [20].

The presence of the solvation force complicates answering the questions that Vergeles *et al.* [3,4] set out to address. To paraphrase: to what extent does Brenner's prediction work at a small length scale, and how is the unphysical divergence of Brenner's solution resolved in a molecular system? The calculations presented in the present paper demonstrate that at a minimum one must consider a range of approach velocities, and consider the variation of the force with the direction of the sphere. The conclusion put forward by Vergeles *et al.*, namely that "Brenner's solution works for most values of h even at a molecular scale," must therefore be considered premature. As this paper shows, for small enough U Brenner's solution must always seriously underpredict the drag force, while for large U the systems studied indicate that it overpredicts. By restricting the simulations to some very large U [21], Vergeles *et al.* [3,4] inadvertently obscured some important issues and insights that can be illustrated with MD simulations.

Among significant insights, we count the decomposition of the drag force. This approach gives a direct indication of the presence of a static contribution and a dynamic contribution that is, like the hydrodynamic contribution, antisymmetric. The suggested decomposition of the drag force is quite general and satisfies obvious requirements. For example, for a hypothetical system of a sphere subject to the sum Brenner's force and a direct wall-sphere force, the decomposition is exact. The decomposition proposed here can be applied to any sphere-wall data whether generated numerically or experimentally. It should prove to be particularly useful in the analysis of experimental measurements of moving AFM or IFM probes. If the experiment can be performed by moving a sphere both in and out, then Eqs. (14) and (15) at a minimum provide an internal consistency check on the data.

ACKNOWLEDGMENTS

We thank Marc Ingber, Jack Houston, Peter Feibelman, John Curro, Jim Miller, and John Shelnutt for helpful discussions. We are grateful for the computational support that has been provided by the UNM Center for High Performance Computing (HPC@UNM) under Grant No. 2005006. This work is supported in part by the DOE Office of Basic Energy Sciences, Division of Material Sciences and Engineering, the DOE Office of Science's Advanced Scientific Computing Research (ASCR) program in Applied Mathematical Sciences, and by Sandia's LDRD program. Sandia is a multiprogram laboratory operated by Sandia Corporation, a Lockheed-Martin Company, for the U.S. DOE under Contract No. DE-AC04-94AL85000.

[1] G. G. Stokes, Proc. Cambridge Philos. Soc. **9**, 8 (1851).
[2] H. Brenner, Chem. Eng. Sci. **16**, 242 (1961).
[3] M. Vergeles, P. Keblinski, J. Koplik, and J. R. Banavar, Phys. Rev. Lett. **75**, 232 (1995).
[4] M. Vergeles, P. Keblinski, J. Koplik, and J. R. Banavar, Phys. Rev. E **53**, 4852 (1996).
[5] B. J. Alder, W. E. Alley, and E. L. Pollock, Ber. Bunsenges. Phys. Chem. **85**, 944 (1981).
[6] H. T. Davis, *Statistical Mechanics of Phases, Interfaces, and Thin Films* (Wiley-VCH, New York, 1996).
[7] L. J. D. Frink and F. van Swol, J. Chem. Phys. **108**, 5588 (1998).
[8] J. N. Israelachvili, *Intermolecular and Surface Forces* (Academic, New York, 1986).
[9] D. C. Rau and V. A. Parsegian, Biophys. J. **61**, 260 (1992).
[10] Oftentimes the solvation force is known by other or more specific names depending on the field in which it was first described. Thus, besides the solvation force, one can encounter hydration force, depletion interaction, or hydrophobic interaction.
[11] J.-P. Hansen and I. R. McDonald, *Theory of Simple Liquids*, 2nd ed. (Academic Press, Inc., 1986).
[12] M. P. Allen and D. J. Tildesley, *Computer Simulation of Liquids* (Oxford University Press, 1987).
[13] Note, however, that although the choice $b=d/2+\sigma$ appears intuitively appealing for a one-component fluid, it is less clear how to apply it to multicomponent fluids.
[14] W. H. Press, S. A. Teukolsky, W. T. Vetterling, and B. P. Flannery, *Numerical Recipes in FORTRAN: The Art of Scientific Computing*, 2nd ed. (Cambridge University Press, 1992).
[15] In principle it is, of course, always possible to construct a distribution $\mathcal{P}_r(h';\bar{h})$ that would have the special property that $F_{\mathrm{solv}}^{\mathrm{rough}}(\bar{h})=0$ for a certain $\bar{h}$. But this is unlikely to extend to *all* values of $\bar{h}$.
[16] In our figures and simulation results, we will refer to the total force, F_z, as the drag force.
[17] For example, the decoupling introduced here allows one to verify if a superposition approximation is appropriate, by demonstrating that it is independent of U.
[18] G. Drazer, B. Khusid, J. Koplik, and A. Acrivos, Phys. Rev. Lett. **95**, 016102 (2005).
[19] K. J. Tupper and D. W. Brenner, Langmuir **10**, 2335 (1994).
[20] Clearly, it would be of some interest to revisit the effects of molecular wall structure [4] in light of the decoupling technique proposed here. The interplay of static and dynamic force contributions can be highlighted using that strategy. Each con-

tribution can then be analyzed separately to establish how it is affected by the presence of molecular structure. However, we stress that isolating the effects of surface structure is not entirely straightforward. When a structured wall is replaced by a smoothed averaged potential, one inevitably faces certain limitations that originate from exactly how the averaging of the wall-fluid interactions is performed. For example, one can consider the solid wall to have a continuum density and average the potential energy directly. Alternatively, one can define a smooth-wall potential by averaging the Boltzmann factor of structured wall interactions. The latter strategy would ensure that the low-density limit of the density profile and the adsorption is the same for the smooth and the structured wall (see Ref [22]).

[21] We note that the sphere velocities employed in Refs. [3,4] must be considered too high even though *Re* is of order unity due to the small sphere size. $U=2$ implies a sphere velocity that is larger than the average speed of a fluid molecule ($1.75\sqrt{\epsilon/m}$), and of the order of the speed of sound ($5.6\sqrt{\epsilon/m}$). Running a simulation at this U likely results in serious local heating even when a global thermostat is employed. This makes U values of order 1 unsuitable choices to test Brenner's result.

[22] W. A. Steele, *The Interaction of Gases with Solid Surfaces* (Pergamon Press, 1974).